

3D discrete model for thermal contrast enhancement and defects depth estimation in CFRP slabs.

PROCESAMIENTO DIGITAL DE IMÁGENES

Modelo discreto 3d para mejoramiento del contraste térmico y estimación de profundidad de defectos en láminas de CFRP.

Andrés D. Restrepo-Girón*§, Humberto Loaiza-Correa*

**Facultad de Ingeniería, Escuela de Ingeniería Eléctrica y Electrónica,
Universidad del Valle, Cali, Colombia*

§ andres.david.restrepo@correounivalle.edu.co, humberto.loaiza@correounivalle.edu.co

Recibido: Abril 18 de 2013- Aceptado: Enero 28 de 2014

Abstract

Two finite difference discretization approaches of the Fourier's 3D heat propagation model are introduced, from which a new technique is proposed to enhance the thermal contrast of infrared sequences of images acquired from pulsed active thermography experiment for non-destructive testing of CFRP slabs. The discrete models defined are easily adaptable to a spatial filter structure, which can be applied to each image of the infrared sequence to obtain a better contrast between possible internal flaws and sound regions of material, and hence, a better probability of flaws detection. The performance of the technique proposed is evaluated using artificial thermal sequences generated by ThermoCalc6L, software that is able to compute dynamic thermal distributions in anisotropic layered solids, simulating internal defects and different excitation sets. Results show that this technique offers a better contrast between defects and image background than other relevant techniques like modified-differential absolute contrast, and a potentially faster execution than techniques based on thermal distribution reconstruction like the 3D thermal filtering method.

Keywords: *Defects characterization, heat transfer model, Infrared thermography, thermal contrast.*

Resumen

Se introducen dos aproximaciones por diferencias finitas al modelo clásico de Fourier de propagación del calor en 3D a partir de las cuales se propone una nueva técnica para mejorar el contraste térmico en secuencias de imágenes infrarrojas adquiridas a partir de experimentos de termografía activa pulsada para ensayo no destructivo de láminas delgadas de CFRP. Los modelos anteriores se adaptan fácilmente a una estructura de filtro espacial que puede aplicarse a cada imagen de la secuencia con el fin de obtener un mejor contraste entre posibles defectos internos y las regiones sanas del material, y por tanto, una mayor probabilidad de detección. El desempeño de la técnica propuesta se evalúa empleando secuencias artificiales sintetizadas con el software ThermoCalc6L, que permite computar las distribuciones de temperatura en láminas sólidas anisotrópicas, simulando defectos internos y diferentes esquemas de excitación. Los resultados muestran que la técnica propuesta ofrece un mejor contraste térmico que técnicas relevantes como el contraste absoluto diferencial modificado, y una velocidad potencialmente superior de ejecución sobre las técnicas basadas en la reconstrucción de la distribución térmica, como el caso del método de filtrado térmico 3D.

Palabras clave: *Caracterización de defectos, contraste térmico, modelo de transferencia de calor, termografía infrarroja.*

1. Introduction

Although thermography is not an area with recent application in engineering, it has become one of the more promising techniques for *Non-Destructive testing* (NDT) because of non-contact and non-intrusion qualities (Meola, 2004), and advances in informatics and computing systems, which have increased the performance of digital image processing algorithms. So, thermography is gaining relevance in predictive and preventive maintenance activities in automotive and aeronautical industries where the use of composite materials, like *Carbon Fiber Reinforced Plastic* (CFRP), is more and more extended since they exhibit a better mechanical resistance/weight ratio than other very important materials such as aluminum and steel (Snell, 2007). For example, CFRP slabs are included as structural material for flight control surfaces, and fuselages of military and commercial planes, resulting in savings up to 20% of fuel consumption and a decrease of the same quantity in CO₂ emissions (IATA, 2009). However, excessive impacts or repetitive mechanical stress applied to a composite material may create several types of failures, the most common being *delamination* between layers (Pohl, 1998), which may grow until breaking the material.

The *Pulsed Active Thermography* (PT) is one of several techniques created to detect those failures. Despite of the undeniable reliability of ultrasound NDT methods, PT offers the advantage of a remote sensing and a wider area of inspection in one take, helped by the increased quality of infrared cameras. This technique consists of the thermal excitation of the material under evaluation through a high power lighting pulse which width depends on the thermal conductivity. The evolution of temperature, or *thermal profile*, is recorded in a sequence of infrared images or *thermograms*, and attention is focused at how each pixel gets cool with time, because a defective area will cool with more or less speed than a sound area (depending on thermal conductivities). Later, images are subject to a processing procedure named *thermal contrast* (Ibarra, 2005), which pretends to compensate the background temperature distribution and recover only the more contrasted peculiarities or anomalies in the inspected sample.

The main problem in obtaining contrast enhanced images lays in the fact that the excitation heating in PT does not distribute uniformly through the radiated surface, but in real cases, emissivity variability of the material and optical distortions of the IR camera also contribute to this non-uniformity effect. The simplest method of subtracting an arbitrary sound point profile from every point profile, or absolute contrast (AC), is not suitable for this objective; there are refinements of the previous one, the most important being the normalized contrast (NC), that throw better results but have the drawback (at least for automating purposes) of requiring a sound area selection prior to detect where the flaws are, if exist (Benítez, 2011).

In an effort to face this challenge, the *Differential Absolute Contrast* (DAC) method was proposed as a solution to the problem of a priori selection of a sound area; it is based on the 1D model of adiabatic heat transfer over the surface of a solid semi-infinite material without internal flaws, heated by a thermal pulse. The technique pretends to predict the temperature in every sound point of the excited surface to subtract these predicted values from sensed real temperatures, and obtain greater discrepancies from defective regions than from sound areas (Benítez, 2007). The good results for DAC depend mainly on good approximations to a semi-infinite object (case for thick layers) and to a thermal impulse excitation (case for narrow heating pulses). To overcome this disadvantage, the *modified-DAC* (m-DAC) technique was proposed (Benítez, 2008), using a corrected version of the previous 1D heat transfer model derived from *thermal quadrupoles* theory (Maillet, 1993) that works in the complex variable s space for simplicity. The new model introduces the thickness of the layer, the time width of the heating pulse, and diffusivity of the material, attenuating the distortion of thermal profiles introduced by the real shape of the heating pulse and the reflection of the heat wave in the opposite side of a layer. The remaining problem now is about using a 1D model to resolve a 3D problem; but tridimensional methods have a drawback in the computational effort required to reconstruct the thermal distribution inside the evaluated specimen. Nevertheless, the work of Grinzato *et*

al. (2000) is one of the first intentions to involve a 3D heat conduction model in thermal contrast, resulting in the 3D filtering technique that estimates the 3D temperature evolution of healthy material to subtract it from the real one.

The technique proposed in this paper is based on a discretized 3D model of heat diffusion, in such a way it can offer a better thermal contrast and more relative energy profiles than classic techniques, without a sound area, a reference thermogram selection, or a high computational effort. Moreover, it does not depend on theoretical data, but only on experimental thermal data and definition of a few parameters, leading to low sensitivity on simulation parameters values. To illustrate the developing and some results of this technique, two approximations of the discretized model, a new thermal contrast definition and a new depth estimation method, will be shown in chapter 2; the main results and relevant analysis of them are exposed in chapter 3, while final conclusions are treated in chapter 4.

2. Discretization of 3D heat transfer model and new thermal contrast definition

The complete 3D model of heat propagation through a specific medium is given by Eq. (1):

$$\frac{\partial}{\partial x} \left(K_x \frac{\delta T(x,y,z,t)}{\delta x} \right) + \frac{\partial}{\partial y} \left(K_y \frac{\delta T(x,y,z,t)}{\delta y} \right) + \frac{\partial}{\partial z} \left(K_z \frac{\delta T(x,y,z,t)}{\delta z} \right) + W(x,y,z,t) = C\rho \frac{\delta T(x,y,z,t)}{\delta t} \quad (1)$$

where T_i is the temperature excess in the layer i with respect to surround temperature; C_i and ρ_i are specific heat and density of the layer i ; K_{qi} is the thermal conductivity through direction q in the layer i ; $W(x,y,z)$ is the heat generation per volume unity (power density in W/m^3) inside the propagation medium. If we consider that the specimen is an isotropic and homogenous medium, the thermal excitation is very similar to an impulse function, no heat is generating inside the slab, and there is no loses by convection through its surfaces, Eq. (1) can be discretized by finite differences in an explicit way (Restrepo, 2012), as shown:

$$\frac{1}{\alpha} \frac{T_{ijk}^{m+1} - T_{ijk}^m}{\Delta t} = \left(\frac{T_{(i-1)jk}^m - 2T_{ijk}^m + T_{(i+1)jk}^m}{\Delta x^2} \right) + \left(\frac{T_{i(j-1)k}^m - 2T_{ijk}^m + T_{i(j+1)k}^m}{\Delta y^2} \right) + \left(\frac{T_{ij(k-1)}^m - 2T_{ijk}^m + T_{ij(k+1)}^m}{\Delta z^2} \right) \quad (2)$$

Where:

- $t_m = m.\Delta t$, with $m = 0,1,2,\dots,M-1$, being M the total number of thermograms acquired, and Δt , acquisition period of images;
- $x_i = i.\Delta x$, with $i = 0,1,2,\dots,N_x - 1$, being N_x the total number of rows in each image; and $\Delta x = L_x / N_x$, being L_x the vertical length of image field;
- $y_j = j.\Delta y$, with $j = 0,1,2,\dots,N_y - 1$, being N_y the total number of columns in each image; and $\Delta y = L_y / N_y$, being L_y the horizontal length of image field;
- $z_k = k.\Delta z$, with $k = 0,1,2,\dots,N_z - 1$, being N_z the total number of steps dividing the thickness of slab; and $\Delta z = L_z / N_z$, being L_z that thickness. Value of N_z is unknown in a real PT experiment;
- T_{ijk}^m , temperature on pixel i,j,k for thermogram m ;
- $\alpha = \kappa / C\rho$, being the thermal diffusivity of the specimen.

Considering squared pixels: $\Delta x = \Delta y = \Delta p$, and defining a dimensionless parameter: $\beta = \alpha \Delta t / \Delta p^2$, we have:

$$T_{ijk}^{m+1} - T_{ijk}^m = \beta \left[(T_{(i-1)jk}^m - 2T_{ijk}^m + T_{(i+1)jk}^m) + (T_{i(j-1)k}^m - 2T_{ijk}^m + T_{i(j+1)k}^m) \right] + \left(\frac{T_{ij(k-1)}^m - 2T_{ijk}^m + T_{ij(k+1)}^m}{\Delta z^2} \right) \quad (3)$$

Reorganizing and grouping terms, and defining: $\Phi_m^k = T_{(i-1)jk}^m + T_{(i+1)jk}^m + T_{i(j-1)k}^m + T_{i(j+1)k}^m$, the basis estimation equation is finally obtained:

$$T_{ijk}^{m+1} = \left[1 - 2\beta \left(2 + \frac{\Delta p^2}{\Delta z^2} \right) \right] T_{ijk}^m + \beta \left[\Phi_m^k + \frac{\Delta p^2}{\Delta z^2} (T_{ij(k-1)}^m + T_{ij(k+1)}^m) \right] \quad (4)$$

Knowing β , and choosing Δz so that $\alpha \Delta t / (\Delta z^2) < 1/4$ to grant the model stability (Hensen, 1994), the only problem remained is that terms $T_{ij(k-1)}^m$ and $T_{ij(k+1)}^m$ are unknown. So, assuming heating lateral

dispersion is negligible for a thermal propagation of Δz , two approximations are proposed using solutions of Eq. (1) applying Green functions, according to Tadeu & Simões (2006).

2.1. First approximation

The first approximation comes from a slab configuration as the propagation medium. In this case, it can be stated that heat fluxes are null on both sides of the layer, for which the temperature at point x, y, z inside the slab of width h , due to a heat point source placed at x_0, y_0, z_0 , is determined by:

$$T(x, y, z, t) = W \frac{e^{-r_0/4\alpha\tau}}{\rho C (4\pi\alpha\tau)^{3/2}} + \sum_{n=1}^{NS} W \frac{e^{-r_1/4\alpha\tau} + e^{-r_2/4\alpha\tau} + e^{-r_3/4\alpha\tau} + e^{-r_4/4\alpha\tau}}{\rho C (4\pi\alpha\tau)^{3/2}} \quad (5)$$

where:

$$\begin{aligned} r_0 &= (x - x_0)^2 + (y - y_0)^2 + (z - z_0)^2 ; \\ r_1 &= (x - x_0)^2 + (y - y_0)^2 + (z + z_0 + 2h(n-1))^2 ; \\ r_2 &= (x - x_0)^2 + (y - y_0)^2 + (z + z_0 - 2hn)^2 ; \\ r_3 &= (x - x_0)^2 + (y - y_0)^2 + (z - z_0 + 2hn)^2 ; \\ r_4 &= (x - x_0)^2 + (y - y_0)^2 + (z - z_0 - 2hn)^2 \end{aligned}$$

The idea behind the proposed technique is to obtain an estimation that takes into account only the temperature distribution throughout z axis for a Δz displacement, not the whole temperature distribution inside the specimen. Then, Eq. (5) can be rewritten as:

$$T_{(z_k, t_m)} = \frac{W}{\rho C (4\pi\alpha\tau)^{1/2}} \left[e^{-r_0/4\alpha\tau_m} + \sum_{n=1}^{NS} \left(e^{-r_1/4\alpha\tau_m} + e^{-r_2/4\alpha\tau_m} + e^{-r_3/4\alpha\tau_m} + e^{-r_4/4\alpha\tau_m} \right) \right] \quad (6)$$

Where: $r_\xi = r_\xi |_{x=y=x_0=y_0=0}$, with $\xi = 1, 2, 3, 4$.

In previous equations, NS is an arbitrary number of thermal wave reflections to be considered (the smaller diffusivity, the higher NS value). Now, assuming that heat pulse is applied at initial time ($t_0 = 0$) and over the frontal surface ($z_0 = 0$) of the inspected slab, and defining: $\sigma_m = 4\alpha t_m = 4\beta m \Delta p^2$, we can write:

$$T_{ijk}^m = \frac{W}{\rho C (4\pi\alpha t)^{1/2}} [A^{(NS)_k^m}] \quad (7)$$

being: $A^{(NS)_k^m} = e^{-z_k^2/\sigma_m} + \sum_{n=1}^{NS} \left(e^{-(z_k+2h(n-1))^2/\sigma_m} + 2e^{-(z_k-2hn)^2/\sigma_m} + e^{-(z_k+2hn)^2/\sigma_m} \right)$

To eliminate the power density of heating W in the approximation, it can be defined in general that:

$$T_{ij(k\pm 1)}^m = \frac{T_{ijk}^m}{A^{(NS)_k^m}} [A^{(NS)_{k\pm 1}^m}] \quad (8)$$

Replacing Eq. (8) in Eq. (4), we obtain:

$$\tilde{T}_{ijk}^{m+1} = \left\{ 1 - \beta \left[4 + \frac{\Delta p^2}{\Delta z^2} \left(2 - \frac{A^{(NS)_{k+1}^m} + A^{(NS)_{k-1}^m}}{A^{(NS)_k^m}} \right) \right] \right\} T_{ijk}^m + \beta \Phi_k^m \quad (9)$$

Considering that the information from the thermal sensor corresponds to the surface temperature, and the estimation for the next time instant is restricted to the temperature over the surface where $z = 0$ ($k = 0$ in Eq. (9)), we obtain the approximate heat transfer model named *3D differentiated thermal estimation*:

$$\tilde{T}_{ij0}^{m+1} = \left\{ 1 - \beta \left[4 + \frac{\Delta p^2}{\Delta z^2} \left(2 - \frac{A^{(NS)_{(1)}^m} + A^{(NS)_{(-1)}^m}}{A^{(NS)_0^m}} \right) \right] \right\} T_{ij0}^m + \beta \Phi_0^m \quad (10)$$

The restriction imposed to this estimation makes the proposed thermal contrast technique, based on Eq. (10), to be faster than any other method that rebuilds temperature in every point inside the slab.

2.2 Finite difference thermal contrast (FDTC) technique

Terms in Eq. (10) can be placed in a 3×3 filtering mask, where the first term of Eq. (10) would be assigned to the central element, the term β to elements in the 4-neighborhood and zero to corner elements; in such a way the estimation process is converted to a dynamic filtering one. Applying this mask to each thermogram, the next value of temperature (in the time domain) for each pixel is predicted; if $T_{ij0}^{(m+1)}$ and $\tilde{T}_{ij0}^{(m+1)}$ denote the real and the estimated next temperature for a specific pixel in Eq. (11), F_{ij0}^m represents the relative error in

estimation which may be expected to be less for pixels corresponding to healthy zones than that for pixels laying to defective areas, leading to enhanced images.

$$F_{ij0}^m = \frac{T_{ij0}^{m+1} - \tilde{T}_{ij0}^{m+1}}{T_{ij0}^{m+1}} \quad (11)$$

This output represents the relative excess of estimated temperature over the real one. The time evolution of this excess of temperature creates the typical *differential profile* P_D shown in figure 1a. This behaviour is according to an initial slower cooling phase and a later faster cooling phase of defect regions with respect to sound regions (in the case of defect conductivity smaller than layer conductivity). However, for detection purpose it is better to work with accumulated profiles P_A , by means of a summing function over P_D , obtaining curves just similar to those with common enhancement methods (figure 4).

2.3 Second approximation and depth estimation of internal flaws

The second way of approximation to $T_{ij(k\pm 1)}^m$ terms consists in using the Tadeu and Simões model for a semi-infinite medium, explained by Eq. (12), with null normal flux at the surface ($z = 0$):

$$T(x, y, z, t) = W \cdot \frac{e^{-r_0/4\alpha t} + e^{-r_1/4\alpha t}}{\rho C (4\pi\alpha t)^{3/2}} \quad (12)$$

where $r_0 = (x - x_0)^2 + (y - y_0)^2 + (z - z_0)^2$;
 $r_1 = (x - x_0)^2 + (y - y_0)^2 + (z + z_0)^2$.

Taking again the temperature distribution only throughout z axis, applying a heating source at $z_0 = 0$ and $t_0 = 0$, and finally extracting constant terms as in the first approximation, results:

$$\frac{2W}{\rho C (4\pi\alpha)^{1/2} t_m^{1/2}} = T(z_k, t_m) e^{z_k^2/4\alpha t_m} \quad (13)$$

and rewriting:

$$T_{ij(k\pm 1)}^m = T_{ijk}^m e^{(k\Delta z)^2/4\beta m \Delta p^2} e^{-((k\pm 1)\Delta z)^2/4\beta m \Delta p^2} \quad (14)$$

Now, replacing Eq. (14) in Eq. (4), and restricting for temperature data at surface ($k = 0$):

$$\tilde{T}_{ij0}^{m+1} = \left\{ 1 - 2\beta \left[2 + \frac{\Delta p^2}{\Delta z^2} (1 - e^{-\Delta z^2/4\beta m \Delta p^2}) \right] \right\} T_{ij0}^m + \beta \Phi_0^m \quad (15)$$

Figure 1 reveals the differences between profiles obtained with FDTC using Eq. (15) and those given by the first approximation. What is interesting here is that differentials profiles for sound points of material, in figure 1b, do not tend to zero as in figure 1a, but exhibit a positive peak of temperature excess, like defect profiles, as if healthy regions of material were cooling slower than expected; hence, this fact is related with the presence of the back surface of the slab that reflects the thermal wave, as in DAC case, because this reflection would not exist if the medium was semi-infinite. This phenomenon gets more evident if every 2nd approximation profile is subtracted from its corresponding 1st approximation profile (figure 1c), since the resulting profiles are coincide with each other (figure 1d) and remark the maximum of excess temperature due to the back surface presence.

In the work of Gilbert & Mathias (1988) the Laplace transform is used to model a biological system consisting of three layers of human tissue, which together behave as an unique layer in transient state, with an *effective diffusivity* α_{eff} defined by means of *transit time* or *diffusion time* t_{tr} concept (Maldague, 2001). The same idea can be introduced in the layered model for the problem of an internal defect surrounded by sound substrate material (figure 2).

Attending the last scheme in figure 2, about a piece of material (diffusivity α and width z_L) with an internal defect (diffusivity α_d and width z_2), we can define the effective diffusivity in such a way that:

$$\frac{z_L}{\sqrt{\alpha_{eff}}} = \frac{z_1}{\sqrt{\alpha}} + \frac{z_2}{\sqrt{\alpha_d}} + \frac{z_3}{\sqrt{\alpha}} ; \quad z_L = z_1 + z_2 + z_3 \quad (16)$$

But Eq. (16) is equivalent to $\sqrt{t_{tref}} = \sqrt{t_{tr1}} + \sqrt{t_{tr2}} + \sqrt{t_{tr3}}$, and so:

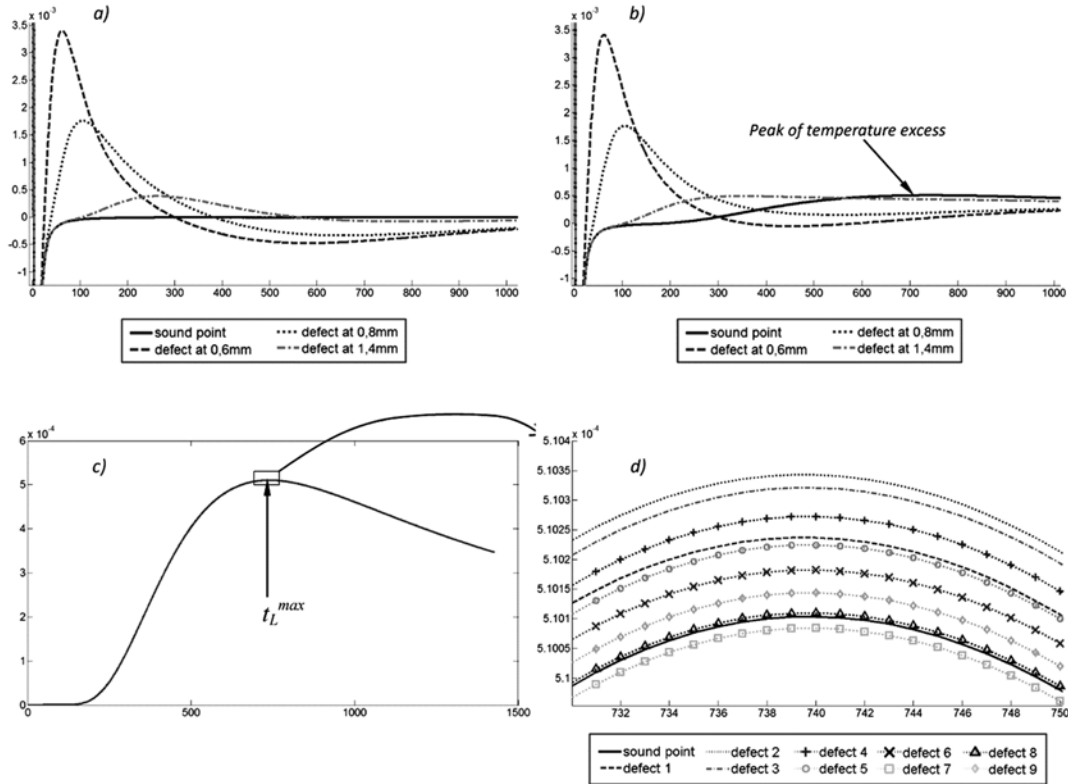


Figure 1. Differential profiles (relative excess of temperature *Vs.* thermogram number) from FDTC: a) profiles obtained with first approximation for three defects with different depths from frontal surface, and one sound point; b) profiles obtained with second approximation; c) resulting coincident curves from 1st and 2nd approximation FDTC differential profiles subtraction for all 9 defects and a sound point; d) zoom of the square around the peak values (the time instants corresponding to peak values are identical)

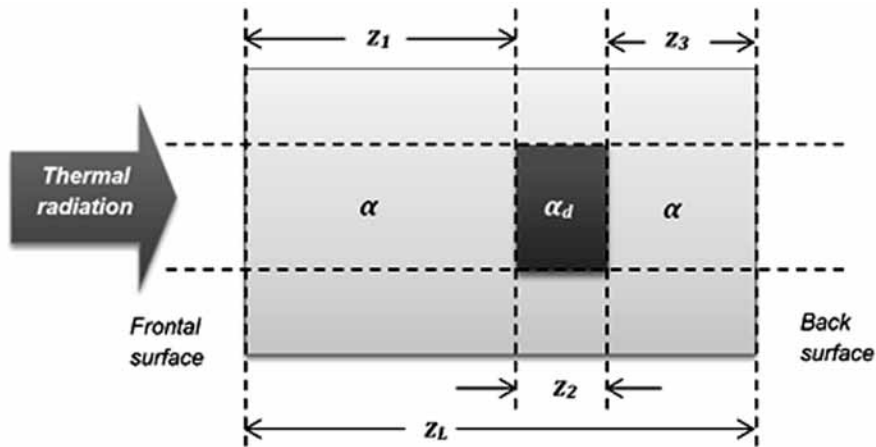


Figure 2. Schematic diagram explaining situation of an internal defect surrounded by healthy material.

$$\frac{\sqrt{t_{tr1}}}{\sqrt{t_{treff}}} = \frac{z_1}{\sqrt{\alpha}} / \frac{z_L}{\sqrt{\alpha_{eff}}} \quad (17)$$

Since a correlation exists between the peaks of differential profiles (equivalent to maximum

derivative points on accumulated profiles PA) and transit times for healthy and defective regions, t_{tr1} and t_{treff} can be replaced by the times where those peaks are found. If we denote these times as t_{dmax} and t_{Lmax} for a defect differential profile

and a healthy area differential profile respectively, and assume very thin flaws ($z_2 \ll z_1 + z_3$), with a large diffusivity compared with that of the slab material ($\alpha_2 \gg \alpha$), we have $\alpha_{eff} \approx \alpha$, and then:

$$z_1 = z_L \sqrt{\frac{t_d^{max}}{t_L^{max}}} \quad (18)$$

3. Results and discussion

3.1. Contrast enhancement

A CFRP slab composed by one layer, was synthesized with ThermoCalc6L software, with an area of 20×20 cm, 2mm thick, and 9 internal squared defects of air, 0.1mm thick and 100 mm^2 of area, each one located at different depths. For simulation purposes, the following parameters were set: $\Delta x = \Delta y = 1$ mm, $\Delta z = 0,1$ mm, $\Delta t = 6,3$ ms, pulse density = $1 \times 10^5 \text{ W/m}^2$, pulse width = 12,6s, a Gaussian dispersion of heating excitation, and a time window of 9s. Figure 3a presents the thermogram at $t = 6$ s, and figures 3b to 3f illustrate the spatial profiles over a straight line crossing the middle three defects of this image, from

the original sequence, NC, m-DAC, FDTC and truncated FDTC (FDTC without offset) sequences. For this figure, FDTC was applied with the 1st approximation, $\Delta x = \Delta y = 1$ mm, $\Delta z = 0,12$ mm, and NS = 10.

As seen in figure 3, NC offers a very good contrast quality, better than that offered for m-DAC, though the last one has as crucial advantage that it does not request the previous selection of a healthy area; however, the DAC techniques depends strongly of the suitable choice of a reference thermogram (González, 2004). In turn, FDTC exhibits a very flat background though it is deviated from zero, and a stronger transition at the interface between healthy areas and defect ones, due to the better lateral compensation achieved with the 3D model. This greater intensity change at the defect-sound area interface assure a more probability of success in detection of flaws. On the other hand, Figure 4 presents the accumulated profiles P_A extracted from the centroids of defects, from NC, m-DAC, FDTC and truncated FDTC sequences. The most relevant fact is that the decay rate of FDTC profiles for defect points, when the flaw depth increases, is less than the

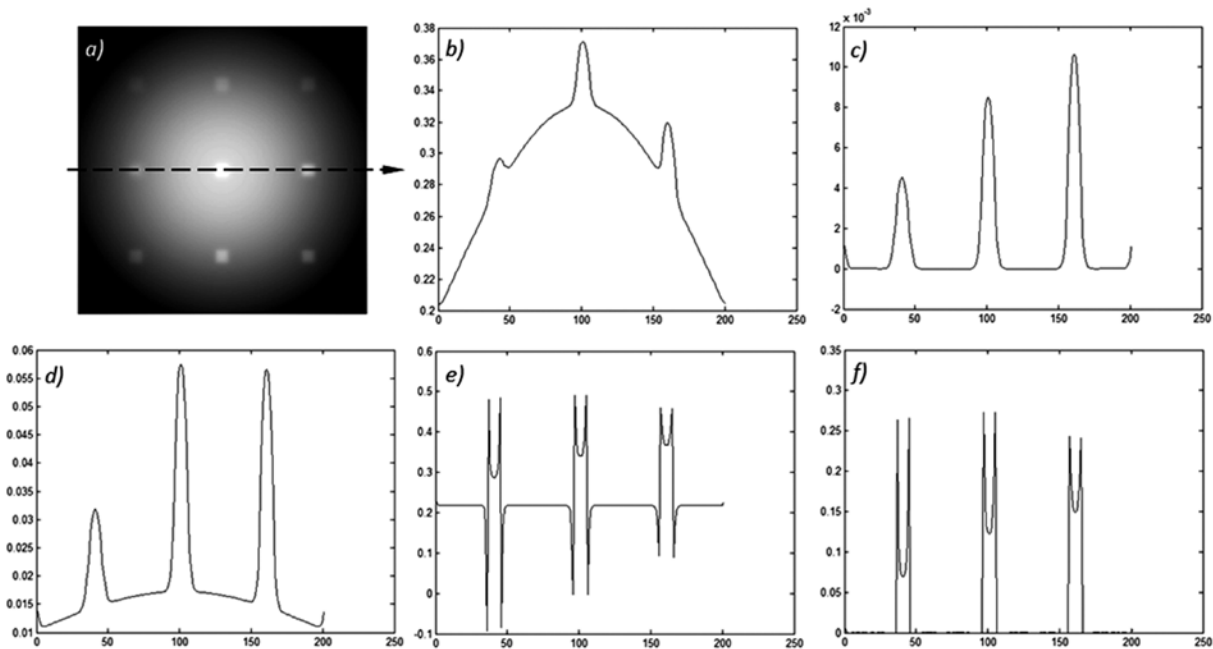


Figure 3. Details about contrast enhancement brought by different techniques: a) the 953th thermogram ($t=6$ s) where the 9 defects are just distinguishable (defects numbers from left to right and up to down: 9-8-7, 1-2-3, 6-5-4); b) original spatial profile coincident with the horizontal line in a); c) NC spatial profile; d) m-DAC spatial profile; e) FDTC spatial profile; f) truncated FDTC spatial profile.

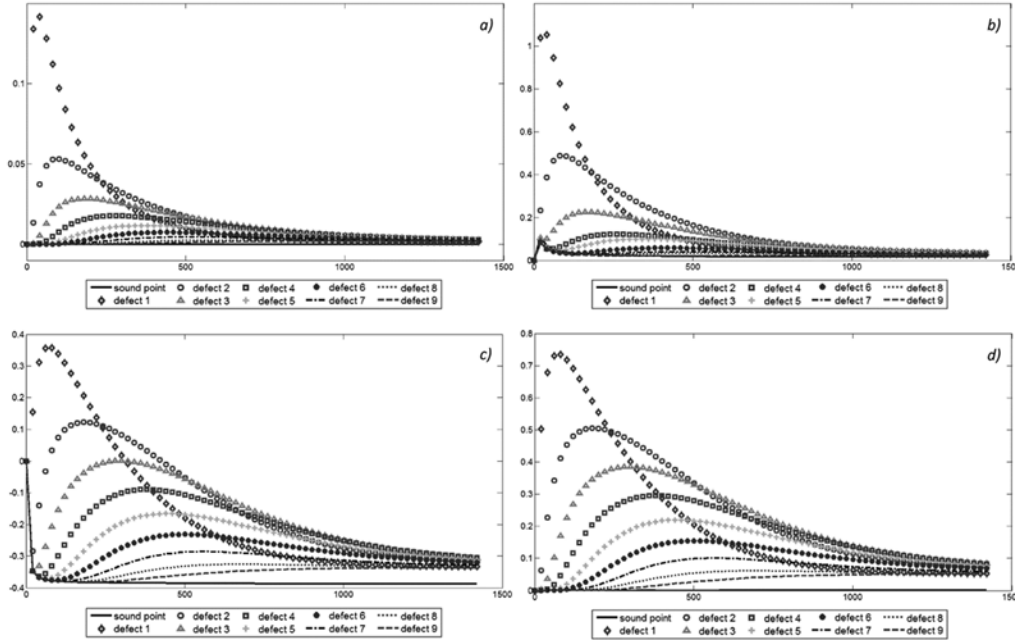


Figure 4. Thermal profiles for all defects and a sound point: a) NC profiles; b) m-DAC profiles; c) FDTC profiles; d) truncated FDTC profiles.

decay rate evidenced in other techniques, which becomes a factor for better global contrast and, as a consequence, a greater probability of defects detection with a smaller diameter/depth ratio.

To measure the residuary background of non-uniformity (inversely proportional to thermal contrast) after application of contrast enhancement techniques, an index of *background relative non-uniformity* is proposed to evaluate how much a contrast enhancement method is able to compensate the non-uniform heating, without concerning if working with profiles represented by temperature quantities or by dimensionless values, as in FDTC and NC. This index is defined for each image by Eq. (19), and relates the intensity span of a thermogram at instant t , $I(t)$, with the intensity span of a sub-image $I(t, p_s)$ constituted by pixels p_s belonging to a subset S of sound regions; additionally, to have a single number to evaluate the global performance of background non-uniformity through a whole sequence, a global index ϑ_g is proposed according to Eq. (20).

$$\vartheta(t) = \frac{\max(I(t, p_s)) - \min(I(t, p_s))}{\max(I(t)) - \min(I(t))}, \forall p_s \in S \quad (19)$$

$$\vartheta_g = \frac{1}{M} \sum_t \vartheta(t) \quad (20)$$

This index (in global fashion or not) can take values between 0 and 1, and behaves inversely to contrast: the closer to zero ϑ (or ϑ_g) is, the more uniform the background is and more thermal contrast the image (or sequence) presents. Table 1 records the values for ϑ_g , demonstrating the better compensation of non-uniformity reached with the proposed method with respect to NC and m-DAC, after an execution time of 2s running in MATLAB on a 3,4 GHz CoreI7 PC with 8 GB RAM.

Table 1. Values of background non-uniformity global index for different cases.

Original	NC	m-DAC	FDTC	Truncated FDTC
0.5404	0.0016	0.1249	7.67x10 ⁻⁶	5.61x10 ⁻⁶

Depth estimation

If the peak time $t_{L,max}$ must be extracted from a P_D for a sound point obtained from the second approximation FDTC model, $t_{d,max}$ must be recovered from a P_D for a defective point obtained

Table 2. Results from application of the depth estimation method proposed.

Defect No.	Real depth [mm]	Estimated depth [mm]	Relative error [%]
1	0,20	0,24	20%
2	0,40	0,40	0%
3	0,60	0,58	3%
4	0,80	0,76	5%
5	1,00	0,92	8%
6	1,20	1,08	10%
7	1,40	1,19	15%
8	1,60	1,28	20%
9	1,80	1,46	19%

from the first approximation *FDTC* model, because defects profiles are not distorted when the slab model is used. Nevertheless, choosing a sound point is a task that must be done after detection of possible defects, and resulting accuracy of depth estimation will depend finally on this selection, over all when there are noise and optical artifacts. A better and more accurate way to find $t_{L,max}$ consists of subtracting a 1st approximation *FDTC* differential profile from a 2nd approximation *FDTC* differential profile, both corresponding to the same pixel, no matter what pixel is chosen as shown in figures 2c and d. Attending this alternative and taking the peak times, $t_{L,max}$ and $t_{d,max}$, table 2 shows results in evaluating Eq. (18) and associated errors. Since profiles are discrete time signals, the previous instants can be replaced by the corresponding integer indexes of thermograms.

4. Conclusions

A contrast enhancement technique named *Finite Differences Thermal Contrast (FDTC)* is defined, based on a proposed discretization of classical heat propagation model in 3D by means of finite differences in an explicit way, and approximations of thermal distribution through a displacement of Δz by applying the 1D solutions proposed by Tadeus & Simoes to 3D transfer differential equation. The first approximation takes the solution for a propagation medium in a slab configuration, assuming null heat fluxes on both sides of the layer; and the second one takes the solution for a semi-infinite medium with null normal flux at the surface. Despite of inducing a distortion in resultant

profiles (similar to classic *DAC*), the last one is useful for implementing an additional proposed simple method for depth estimation of certain flaws based on the corresponding peak time instants on differential profiles; from a simulated *CFRP* slab with air defects, this method shows an error with a maximum value of 20% and a mean about 9%. In both approximations, *FDTC* algorithm does not need to perform temperature estimation in three spatial axes throughout the material in every sample time, making it possible to achieve a substantial reduction in execution time compared to techniques using 3D models for simulation and inversion tasks; but more than this, it can be said that the *FDTC* strategy about contrast enhancement is more reliable than the 3D thermal reconstruction, since the first one estimates temperatures from real values in each thermogram, and the second one performs estimation from ideal initial conditions and theoretical data.

For each pixel and time, *FDTC* gives the relative error of the estimated next temperature with respect to the experimental next temperature over the frontal surface, so that this error increases over defective regions. This feature makes the obtained profiles to be differential and prone to noise, and for that, it is better to work with accumulated profiles to enhance contrast and subsequent defects detection. With respect to *NC* and *m-DAC* techniques, *FDTC* leads to better contrast results according to evaluation of the proposed *global non-uniformity index*, basically due to two principal aspects: the relative energy of thermal profiles in time space is greater than that for *NC* and *DAC* profiles; and the average intensity and

flatness of residual background heating is similar to those resulting from *NC* application, but without the previous selection of a sound area. In real cases, and even though bad pixels correction (Restrepo, 2010) and filtering techniques are used, noise and optical distortions may cause residual background to be less flat and close to zero; but the relative energy of *FDTC* profiles will be preserved, and background irregularity can be compensated with other methods like in Restrepo & Loaiza (2013).

5. Acknowledgements

Authors thank to COLCIENCIAS for the scholarship granted to advance doctoral studies, through its *National PhD Program*; to engineer Hernán Darío Benítez, PhD., and the research Group in *Multipolar Infrared Vision Infrarouge Multipolaire (MIVIM)* from University Laval in Quebec, for infrared thermal image files and for their advice; also, to the *PhD Program in Engineering and Postgraduate Program in Electrical and Electronic Engineering (PPIEE)* at Universidad del Valle.

6. References

- Benítez, H., Ibarra-Castanedo, C., Bendada, A., Maldague, X., Loaiza, H., & Caicedo, E. (2007) Procesamiento de imágenes infrarrojas para la detección de defectos en materiales. *TECNURA*, 10 (20), 40-51.
- Benítez, H., Ibarra-Castanedo, C., Bendada, A., Maldague, X., Loaiza, H., & Caicedo, E. (2008) Definition of a new thermal contrast and pulse correction for defect quantification in pulsed thermography. *Infrared Physics and Technology journal*, 51, 160-167.
- Benítez, H., Loaiza, H., & Caicedo, E. (2011). *Termografía Activa Pulsada en Inspección de Materiales. Técnicas Avanzadas de Procesado*. Cali, Colombia: Universidad del Valle / Universidad Javeriana Ed.
- Gilbert, S., & Mathias, R. (1988). Analysis of diffusion delay in a layered medium: application to heat measurements from muscle. *Biophysical Journal*, 54, 603-610.
- González, D., Ibarra-Castanedo, C., Pilla, M., Klein, M., López-Higuera, J., & Maldague, X. (2004). Automatic Interpolated Differentiated Absolute Contrast Algorithm for the Analysis of Pulsed Thermographic Sequences. In *Proceedings 7th Conference Quantitative Infrared Thermography*, Belgium.
- Grinzato, E., Bison, P., Marinetti, S., & Vavilov, V. (2000). Thermal NDE enhanced by 3D numerical modeling applied to works of art. In *Proceedings of 15th World Conference on Nondestructive Testing*, Italy.
- Hensen, J., & Nakhi, A. (1994). Fourier and Biot numbers and the accuracy of conduction modeling. In *Proceedings of BEP'94 Conference "Facing the Future"*, York, p. 247-256.
- IATA (International Air Transport Association). (2009). *A global approach to reducing aviation emissions. First stop: carbon-neutral growth from 2020*. Switzerland.
- Ibarra, C. (2005). *Quantitative Subsurface Defect Evaluation by Pulsed Phase Thermography: Depth Retrieval with the Phase*. Doctoral Thesis, Faculty of Sciences and Engineering, University Laval. Quebec, Canada.
- Maillet, D., Houlbert, A., Didierjean, S., Lamine, A., & Degiovanni, A. (1993). Non-destructive thermal evaluation of delaminations in a laminate: part I – Identification by measurement of thermal contrast. *Composites Science and Technology*, 47, 137-153.
- Maldague, X. (technical editor). (2001). *Infrared and Thermal Testing. Nondestructive Testing Handbook, Volume 3*. American Society for Non Destructive Testing.
- Meola, C., Carlomagno, G., & Giorleo, G. (2004). Using infrared thermography to analyze substrate and adhesive effects in bonded structures. *Journal of Adhesion Science and Technology* 18 (6), 617-634.
- Pohl, J. (1998). Ultrasonic Inspection of Adaptive CFRP-Structures. *NDT Database & Journal*, 3 (9), *Proceedings of 7th European Conference on Nondestructive Testing*, Denmark.

Restrepo, A., & Loaiza, H. (2010). A new algorithm for detecting and correcting bad pixels in infrared images. *Ingeniería e Investigación*, 30 (2), 197-207.

Restrepo, A., & Loaiza, H. (2012). Modelo de Estimación Diferencial de la Propagación Térmica en 3D mediante Diferencias Finitas. *Sistemas y Telemática*, 10 (21), 9-26.

Restrepo, A., & Loaiza, H. (2013). Non-uniform heating compensation for sequences of thermal images using median filtering. *DYNA* 80 (182), 74-82.

Tadeu, A., & Simões, N. (2006). Three-dimensional fundamental solutions for transient heat transfer by conduction in an unbounded medium, half-space, slab and layered media. *Engineering Analysis with Boundary Elements*, 30, 338-349.